


## $C^{6+}$ -impact ionization of uracil at MeV/u impact energies: The role of the multiple-ionization channel

N. D. Cariatore ,\* N. Bachi , and S. Otranto 

*Instituto de Física del Sur (IFISUR), Departamento de Física, Universidad Nacional del Sur (UNS), CONICET,  
Av. L. N. Alem 1253, B8000CPB-Bahía Blanca, Argentina*

 (Received 20 April 2022; accepted 29 June 2022; published 14 July 2022)

In this work, total and differential ionization cross sections of uracil ionized by  $C^{6+}$  projectiles are calculated by extending an adaptative classical trajectory Monte Carlo model recently introduced in the ion- $H_2O$  collisions context. Calculated cross sections are contrasted and benchmarked against available experimental and theoretical data at impact energies in the MeV/u range. Present results are found in good agreement with the reported experimental data at different levels of differentiability. In addition, the electron emission contributions arising from single and multiple electron ionization are explicitly determined and their partial dominance analyzed in terms of the specific angular and/or energetic ranges.

DOI: [10.1103/PhysRevA.106.012808](https://doi.org/10.1103/PhysRevA.106.012808)

### I. INTRODUCTION

Despite their inherent interest from a basic science perspective, collision processes between highly charged ions and molecules have been widely studied for decades due to their potential relevance in the astrophysical, fusion plasmas, and radiotherapy fields among others. Regarding specifically to the hadrontherapy field, electron emission cross sections of different degrees of differentiability are currently used in simulation codes designed to optimize the irradiation planning stage [1–4]. While most of the operational therapeutical facilities deal with protons as projectiles, highly charged ions are expected to have a higher relative biological effectiveness at the Bragg peak, the region at which most of the dose is delivered. However, this advantage is tempered, for increasing projectile charges, by a dose tail that extends forward into the tissue beyond the Bragg peak. At present,  $C^{6+}$  stands as the optimal projectile to be used with 13 facilities in operational state, five under construction and two in planning stage worldwide [5].

Ionization of  $H_2O$  by highly charged ion impact has been intensively studied, either experimentally or theoretically, during the last decade [6–14]. Regarding RNA bases, uracil ( $C_4H_4N_2O_2$ ) has been analyzed at the total, single differential, and double differential level [14–22]. Theoretical ionization cross sections were calculated by means of the first Born approximation with correct boundary conditions (CB1), the continuum-distorted-wave eikonal initial state (CDW-EIS) [19], the classical over-barrier classical trajectory Monte Carlo method (COB-CTMC) [23], the multicenter CTMC approach [21], and the independent atom model-pixel counting method (IAM-PCM) [14,22]. CTMC cross sections for multiple ionization processes employed in Monte Carlo track structure codes usually make use of the binomial statistical rule and are based on one-electron probabilities [6]. This line

of work within the CTMC method, has been pushed further for  $H_2O$  molecules by considering a dynamical number of frozen electrons in the O and H atomic centers [12,13]. In the IAM-PCM method, the total net ionization cross section for each of the atomic constituents of biologically relevant molecules is translated into a geometrical radius. Under a given molecular orientation, these radii are used to weight the contribution of each atomic center to the net ionization cross section of different biologically relevant molecules, including uracil, based on a geometrical overlap criterion.

In a recent work, we have introduced an adaptative CTMC model (Ad-CTMC) to study collisions of highly charged ions with  $H_2O$  [10]. In this model, eight noninteracting electrons were separately evolved by using a multicenter potential that describes the interaction among one electron and the mean field created by the nuclei and the rest of the electrons of the molecule. The target was dynamically adapted assuming vertical energetic transitions whenever an electron was removed. As a result, the model considered a correct electron density for the valence molecular orbitals, and at the same time required the proper energy deposition by the projectile for multiple electron removal. For  $C^{6+}$  projectiles, and at an impact energy of 4 MeV/u, it was found that while single ionization provided the dominant contribution of low-energy electrons, the largest fraction of electrons with energies greater than about 60 eV were produced in multiple ionization events. For increasing projectile charges ( $O^{8+}$  and  $Si^{13+}$ ), the dominance of multiple ionization vs single ionization was attained at even lower emission energies.

In this work, we extend the Ad-CTMC model to analyze  $C^{6+}$  collisions on uracil ( $C_4H_4N_2O_2$ ) at MeV/u impact energies. Total and differential ionization cross sections are benchmarked against the reported experimental and theoretical data. The separate contributions from the single ionization and the multiple ionization channels are identified and are explicitly shown. Similarities and differences between uracil and  $H_2O$ , in terms of impact parameter distributions are analyzed based on their different molecular geometries. The

\*nelson.cariatore@uns.edu.ar

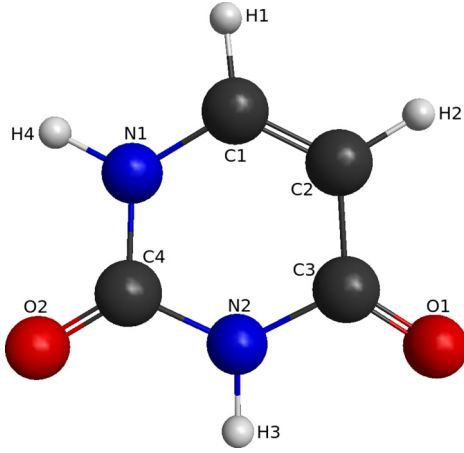


FIG. 1. Geometrical description of the uracil molecule ( $C_4H_4N_2O_2$ ).

organization of the paper is as follows. In Sec. II we describe the present theoretical model. In Sec. III we present the obtained cross sections and benchmark our results against the reported experimental, as well as previous theoretical treatments. Impact parameter distributions for the single and multiple ionization channels are analyzed. Finally, in Sec. IV, conclusions and outlook are drawn. Atomic units are used throughout this work unless otherwise stated.

## II. THEORETICAL METHOD

Within the CTMC method, multicentric descriptions for molecular targets are scarce. One-active electron treatments have been used for  $H_2O$  [12,13,24], and a similar approach

has been recently introduced by Sarkadi for the target considered in this work [21]. In both cases, the active electron is considered to evolve in the target under the mean field created by the nuclei and the rest of the electrons of the molecule via a multicenter potential. Hereafter, we will generically refer to these models as IMC-CTMC. Multielectronic descriptions for molecules have been only reported for  $H_2$  [25–28],  $CO$  [29], and  $H_2O$  [10] up to our knowledge.

In the present Ad-CTMC method, the molecular orbitals and the ionization potentials of the uracil molecule are provided by the GAMESS software by means of a linear combination of Gaussian functions centered at the different atomic centers conforming the molecule (the denominated 6-31G\*\* base) in a restricted Hartree-Fock (RHF) treatment [30]. In Fig. 1 we show the geometrical description of the uracil molecule and label each of its atomic constituents. Mulliken population expansions for the 21 orbitals considered in this work are explicitly tabulated in Table I.

At the beginning of the simulation, and for each molecular orbital, an electron is sorted between the molecular centers based on Mulliken’s populations. The microcanonical procedure is employed at this stage [31]. In this sense, each electron interacts with only one center  $j$  of the molecular orbital as long as it remains bound. This interaction is represented via the potential parametrization developed by Garvey *et al.* [32] based on Hartree-Fock calculations,

$$V_{Gq}(r_{ij}) = -\frac{Z_j - (N_j - 1)(1 - \Omega_j(r_{ij}))}{r_{ij}} \quad (1)$$

$$\Omega_j(r_{ij}) = \left[ \left( \frac{\eta_j}{\xi_j} \right) (e^{\xi_j r_{ij}} - 1) + 1 \right]^{-1}, \quad (2)$$

TABLE I. Mulliken population and binding energies of the uracil molecular orbitals.

Molecular orbital	Mulliken population <sup>a</sup>	Binding energy (a.u.)
1	0.42 C2 + 0.16 C1 + 0.10 O1 + 0.23 N1 + 0.01 C4 + 0.08 O2	−0.362
2	0.02 C3 + 0.45 N2 + 0.26 O1 + 0.01 C4 + 0.25 O2 + ...	−0.418
3	0.04 C3 + 0.07 C2 + 0.07 N2 + 0.01 C1 + 0.61 O1 + 0.01 N1 + 0.02 C4 + 0.16 O2 + ...	−0.433
4	0.02 C3 + 0.03 C2 + 0.04 N2 + 0.02 C1 + 0.13 O1 + 0.05 N1 + 0.05 C4 + 0.63 O2 + 0.01 H3 + 0.02 H1	−0.466
5	0.10 C2 + 0.10 N2 + 0.22 C1 + 0.27 N1 + 0.07 C4 + 0.23 O2 + ...	−0.522
6	0.26 C3 + 0.02 C2 + 0.08 N2 + 0.35 O1 + 0.14 N1 + 0.06 C4 + 0.09 O2	−0.569
7	0.12 C3 + 0.24 C2 + 0.06 N2 + 0.06 C1 + 0.13 O1 + 0.05 N1 + 0.03 C4 + 0.08 O2 + 0.15 H2 + 0.03 H3 + 0.05 H1	−0.596
8	0.10 C3 + 0.13 C2 + 0.04 N2 + 0.11 C1 + 0.36 O1 + 0.05 N1 + 0.04 C4 + 0.08 O2 + 0.05 H2 + 0.02 H1 + 0.03 H4	−0.603
9	0.01 C3 + 0.15 C2 + 0.06 C1 + 0.02 O1 + 0.04 N1 + 0.13 C4 + 0.47 O2 + 0.08 H2 + 0.02 H1 + 0.01 H4 + ...	−0.641
10	0.07 C3 + 0.03 C2 + 0.23 N2 + 0.06 C1 + 0.04 O1 + 0.23 N1 + 0.21 C4 + 0.12 O2 + ...	−0.666
11	0.09 C3 + 0.04 C2 + 0.08 N2 + 0.07 C1 + 0.36 O1 + 0.09 N1 + 0.05 C4 + 0.13 O2 + 0.02 H3 + 0.02 H1 + 0.05 H4	−0.672
12	0.02 C3 + 0.02 C2 + 0.23 N2 + 0.28 C1 + 0.01 O1 + 0.09 N1 + 0.03 C4 + 0.03 O2 + 0.10 H3 + 0.17 H1 + 0.02 H4	−0.713
13	0.14 C3 + 0.15 C2 + 0.12 N2 + 0.13 C1 + 0.06 O1 + 0.18 N1 + 0.13 C4 + 0.05 O2 + 0.01 H1 + 0.01 H4 + ...	−0.771
14	0.04 C3 + 0.17 C2 + 0.18 N2 + 0.07 C1 + 0.01 O1 + 0.28 N1 + 0.01 C4 + 0.02 O2 + 0.08 H2 + 0.05 H3 + 0.09 H4	−0.808
15	0.16 C3 + 0.04 C2 + 0.32 N2 + 0.04 C1 + 0.07 O1 + 0.12 N1 + 0.16 C4 + 0.05 O2 + 0.05 H4	−0.900
16	0.12 C3 + 0.11 C2 + 0.11 N2 + 0.19 C1 + 0.02 O1 + 0.22 N1 + 0.10 C4 + 0.02 O2 + 0.01 H2 + 0.04 H3 + 0.06 H1	−0.932
17	0.09 C3 + 0.38 C2 + 0.02 N2 + 0.27 C1 + 0.02 O1 + 0.10 N1 + 0.04 C4 + 0.02 O2 + 0.03 H2 + 0.02 H1 + 0.01 H4	−1.094
18	0.05 C3 + 0.52 N2 + 0.04 C1 + 0.08 O1 + 0.17 N1 + 0.06 C4 + 0.02 O2 + 0.04 H3 + 0.02 H4	−1.246
19	0.01 C3 + 0.05 C2 + 0.08 N2 + 0.08 C1 + 0.04 O1 + 0.43 N1 + 0.07 C4 + 0.22 O2 + 0.02 H4	−1.317
20	0.19 C3 + 0.01 C2 + 0.04 N2 + 0.59 O1 + 0.01 N1 + 0.03 C4 + 0.13 O2	−1.413
21	0.03 C3 + 0.02 C2 + 0.15 N2 + 0.06 O1 + 0.13 N1 + 0.19 C4 + 0.41 O2 + 0.01 H3 + 0.01 H4	−1.445

<sup>a</sup>Symbol “...” denotes probabilities less than 1%, that were not taken into account in this work.

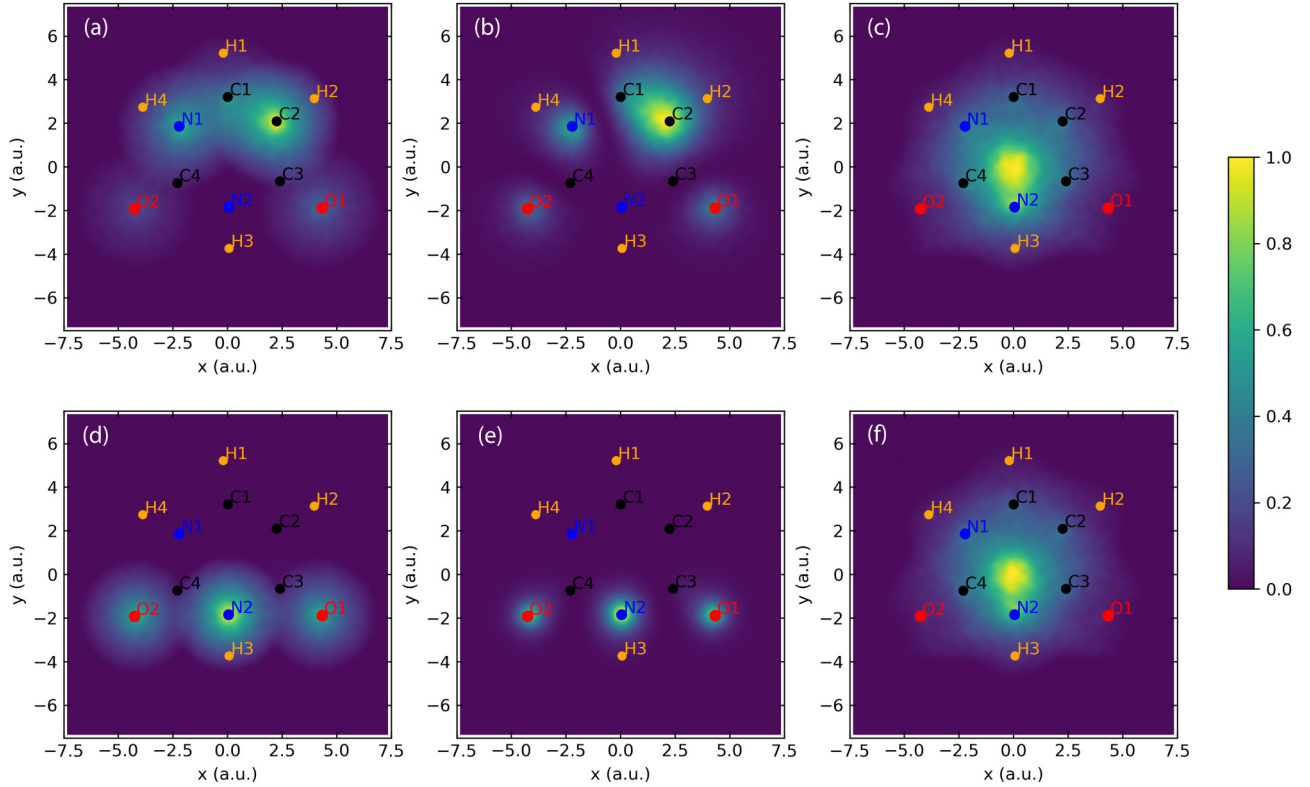


FIG. 2. Electronic densities in the molecular plane for the first orbital (first row) and second orbital (second row) of ground-state uracil. *a* and *d*) present Ad-CTMC method, *b*) and *e*) quantum mechanical description [30], *c*) and *f*) 1MC-CTMC method [21].

where  $Z_j$  is the nuclear charge of the molecular orbital center  $j$ ,  $N_j - 1$  is the corresponding number of screening electrons and  $r_{ij}$  is the distance between an electron  $i$  and the center  $j$ . The parameters  $\xi_j$  and  $\eta_j$  are those tabulated by Garvey *et al.* and are proper of the atom conforming the  $j$  center (C, N, O, or H). The subindex  $q$  denotes the asymptotic charge of center  $j$  as seen by the electron  $i$ . The case  $q = 1$  corresponds to  $N_j = Z_j$  while  $q = 0$  corresponds to  $N_j = Z_j + 1$ .

The electronic orbitals are statistically recovered as the number of sorted trajectories becomes large. This methodology has been used in our previous studies for CO target [29], and seeks a more realistic description of the electron densities in the target. In Fig. 2 we show the electron density obtained in the molecular plane for the first orbital (IP =  $-0.362$  a.u.) and second orbital (IP =  $-0.418$  a.u.) of ground state uracil. The statistical description obtained with the present method is compared to the quantum mechanical description obtained from the molecular orbital wave functions calculated by means of GAMESS and to the classical description obtained within the 1MC-CTMC method [21]. It can be noticed that the present classical description is in good agreement with the quantal description. The main difference observed is the lack of nodal structures in the classical description, together with more circular-shaped structures. In contrast, the 1MC-CTMC method has a notorious electron density concentration at the origin and an amorphous geometric distribution. This is due to the fact that in this model the considered electron interacts with all the atomic centers of the molecule at all times.

A total number of 21 electrons (one per orbital) is explicitly considered. The consideration of the 42 electrons present in orbitals 1–21 in ground-state uracil is prohibitive at present, due to the computational cost involved. After the preliminary initialization of the molecule, the whole system is randomly oriented via an Euler rotation, keeping its center of mass at the origin of the laboratory system. Molecular centers are considered to be fixed in space during the whole simulation.

The electronic Hamiltonian for electron  $i$  is given by,

$$H_i = \frac{p_i^2}{2} + V_{G1}(r_{ij}) - \frac{Z_P}{r_{iP}}. \quad (3)$$

Here,  $p_i$  is the momentum of electron  $i$ , and the last term of the right-hand side of Eq. (3) corresponds to the interaction of the electron with the incident projectile of charge  $Z_P$ .

As the simulation proceeds, Hamilton equations are numerically solved by an adaptive fourth-order Runge-Kutta-Gill method. As it stands, the methodology would clearly lead to the overestimation of the multiple ionization channel, since the amount of energy needed for a given multiple ionization event would underestimate the correct physical value. This is in fact expected for any CTMC model based on  $n$ -independent electrons (nCTMC), which are initialized according to the ground-state energies. The denominated sequential version of the nCTMC model focuses on a more appropriate description of the multiple electron removal processes [33–35]. Here, electrons are sorted according to their sequential binding energies assuming vertical transitions between the different molecular ionic states. While multiple-electron removal is reached with the correct energy deposition by the projectile,

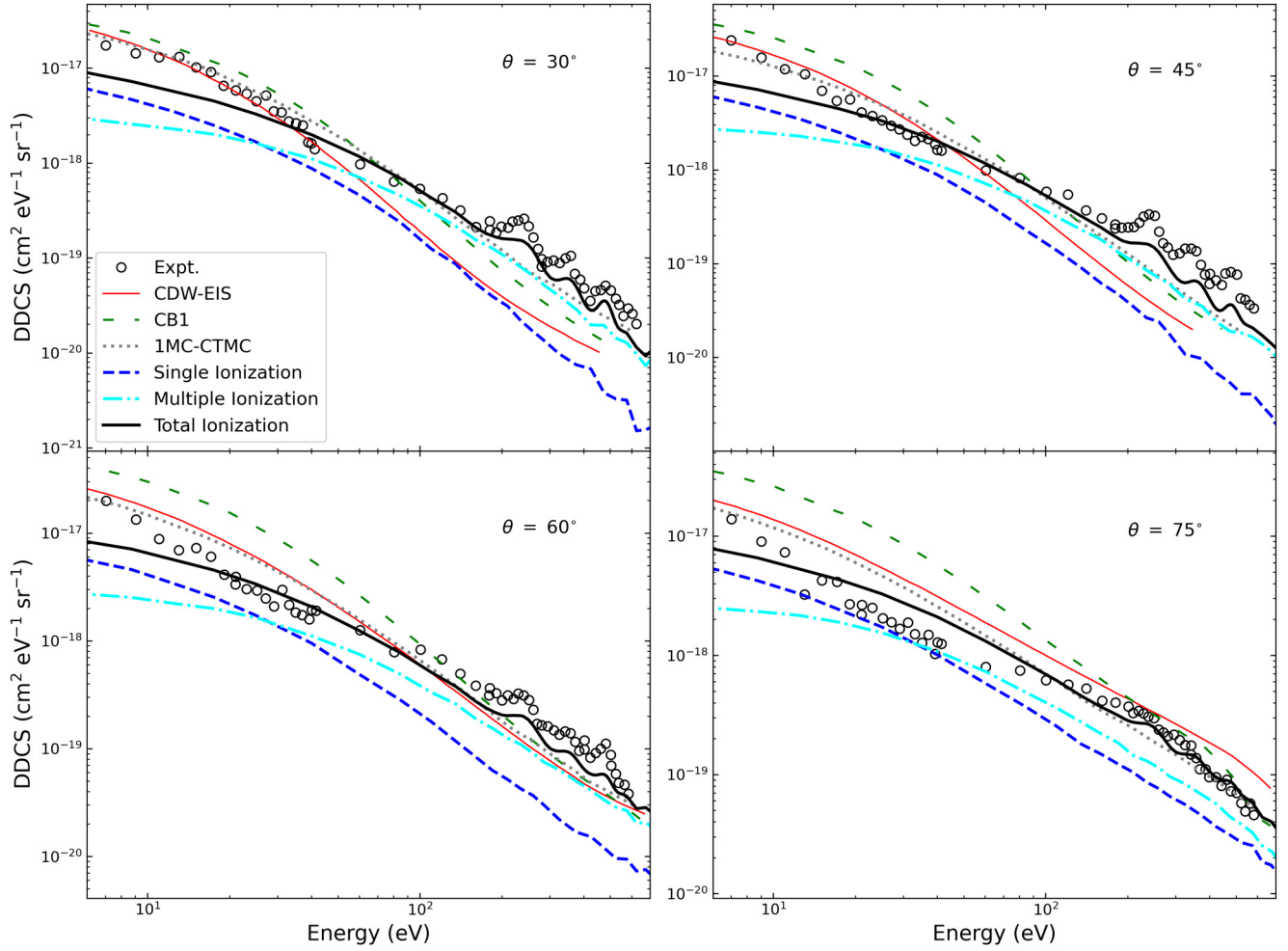


FIG. 3. DDCS as a function of energy at different emission angles. Theories: red thin-solid line: CDW-EIS, green thin-dashed line: CB1, gray dotted line: IMC-CTMC Ref. [21], blue dashed line: Ad-CTMC (single ionization contribution), cyan dash-dotted line: Ad-CTMC (multiple ionization contribution), black solid line: total Ad-CTMC. Auger contributions are incorporated at this point as indicated in the text. The experimental data corresponds to Agnihotri *et al.* [19].

the electron density of the molecular ground state (and the subsequent ionic states) is underestimated in this case. As it was stated above, in a previous work for  $\text{H}_2\text{O}$  we have recently introduced an adaptive dynamical scheme that requires the proper energy deposition by the projectile in order to achieve multiple electron removal [10], and retains at the same time the correct electron density for a given ionic state. In what follows, we briefly describe the electronic rearrangement mechanism, as it applies for the present case.

At each step during the Ad-CTMC simulation, and for each electron, we keep track of the electrons' energies  $E_{ij}$  with respect to their corresponding  $j$  center in the laboratory system:

$$E_{ij} = \frac{p_i^2}{2} + V_{G1}(r_{ij}), \quad (4)$$

For reasons detailed below, we also keep continuous track for each electron of their energy in case they were also interacting with the rest of the centers in their corresponding molecular orbital via asymptotically neutral Garvey potentials

$[V_{G0}(r_{ik})]$ ,

$$E_i^{orb} = \frac{p_i^2}{2} + V_{G1}(r_{ij}) + \sum_{\substack{k=1 \\ k \neq j}}^{NCO} V_{G0}(r_{ik}). \quad (5)$$

Whenever an electron acquires energies  $E_i > 0$  and  $E_i^{orb} > 0$ , the electron is assumed to have been emitted and the interactions between the electron and the remaining nuclei of the molecular orbital are explicitly turned on. As a result the new Hamiltonian under which that electron evolves is given by

$$H_i = \frac{p_i^2}{2} + V_{G1}(r_{ij}) + \sum_{\substack{k=1 \\ k \neq j}}^{NCO} V_{G0}(r_{ik}) - \frac{Z_P}{r_{iP}}. \quad (6)$$

Here,  $NCO$  represents the number of atomic centers in a given molecular orbital. The double requirement  $E_i > 0$  and  $E_i^{orb} > 0$  rules out the possibility that the electron could be recaptured by the target itself, once the other molecular centers conforming to the molecular orbital are turned on. Simultaneously, the remaining target electrons are resorted anew

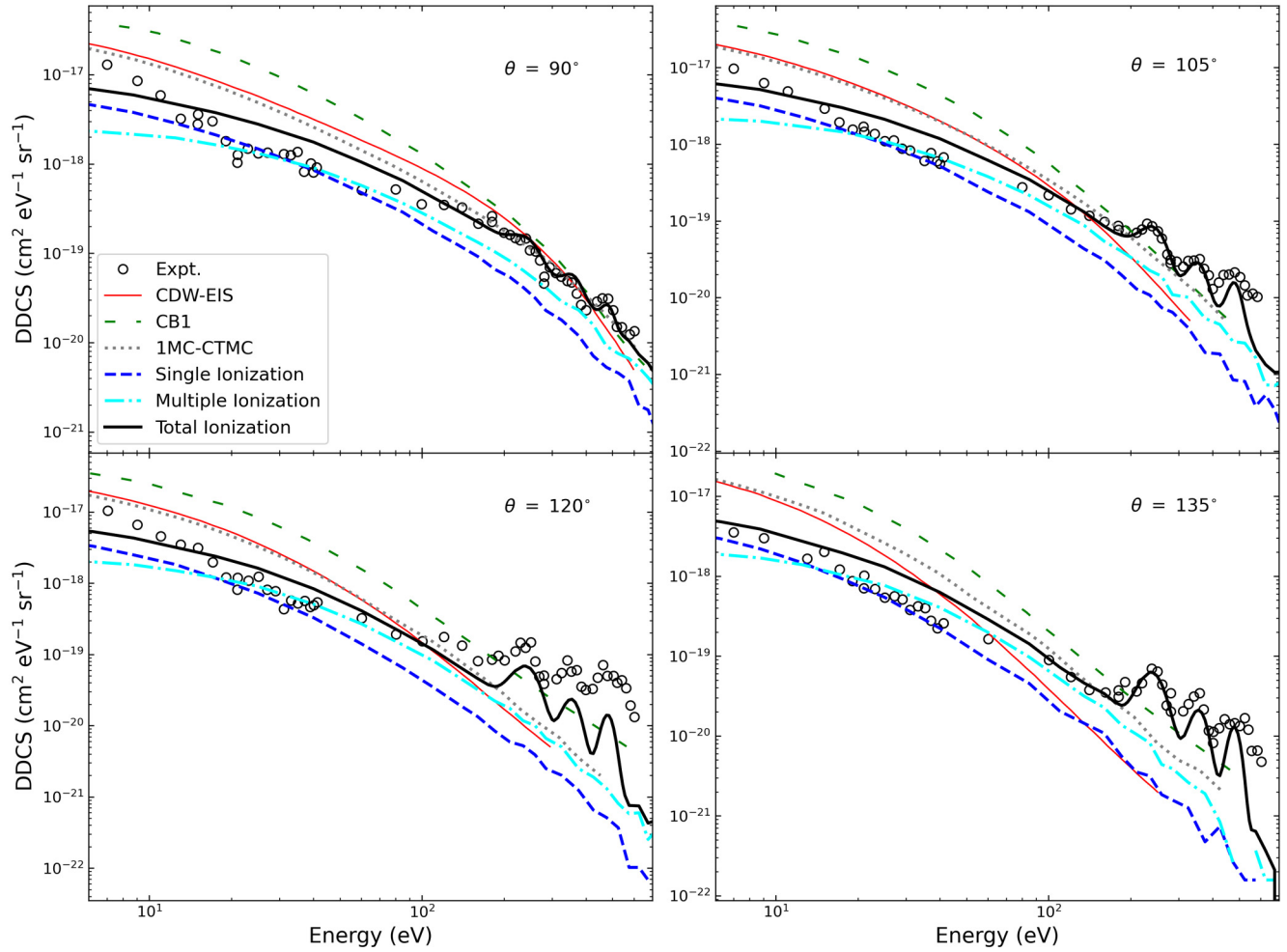


FIG. 4. DDCS as a function of energy at different emission angles. Theories and experimental data as in Fig. 3.

assuming vertical energetic transitions to the new molecular orbitals for the molecular ion. These new molecular orbitals are calculated through the GAMESS software similarly as detailed above. Again, electrons are sorted in the molecular orbitals for the uracil<sup>+</sup> ion according to their Mulliken populations. The whole process is then repeated as more electrons are eventually removed from the target. By doing so, the molecular contraction dynamics that follows each electron removal event is explicitly considered in the collisional dynamics. Molecular orbitals for uracil ions with odd charge state were calculated by means of the restricted-open-shell-Hartree-Fock method (ROHF), and those with even charge state by the RHF method.

Double differential ionization cross sections (DDCS) as a function of the electron energy and emission angle are calculated as:

$$\frac{d\sigma_{\text{net}}}{d\epsilon d\Omega} = \frac{N_{\text{ion}}(E_i, \theta_i)}{N_{\text{tot}}} \frac{1}{\Delta E_i} \frac{1}{\Delta \Omega} \pi b_{\text{max}}^2. \quad (7)$$

Here,  $N_{\text{ion}}(E_i, \theta_i)$  is the number of ionization events with emission energy  $E_i$  and emission angle  $\theta_i$ ,  $N_{\text{tot}}$  is the total number of trajectories considered,  $b_{\text{max}}$  is the maximum impact parameter, and  $\Omega$  is the solid angle where the electronic emission is measured. Since one electron has been considered per orbital, ionization events from an orbital with a state of

occupancy equal to 2 are duplicated at this point. The same statement applies for the lesser order differential cross sections that will now be described.

Singly differential cross sections (SDCS) in energy and angle are calculated as follows:

$$\begin{aligned} \frac{d\sigma_{\text{net}}}{d\epsilon} &= \frac{N_{\text{ion}}(E_i)}{N_{\text{tot}}} \frac{1}{\Delta E_i} \pi b_{\text{max}}^2, \\ \frac{d\sigma_{\text{net}}}{d\Omega} &= \frac{N_{\text{ion}}(\theta_i)}{N_{\text{tot}}} \frac{1}{\Delta \Omega} \pi b_{\text{max}}^2, \end{aligned} \quad (8)$$

and the total ionization cross section (TCS) is given by

$$\sigma_{\text{net}} = \frac{N_{\text{ion}}}{N_{\text{tot}}} \pi b_{\text{max}}^2. \quad (9)$$

Since the asymptotic momenta of all the emitted electrons are explicitly analyzed for each ionization event, and we keep track of the orbital they come for along with the occupancy, the separation of the single and multiple ionization contributions in Eqs. (7)–(9) is straightforward. In all cases, *net* cross sections have been considered ( $\sigma_{\text{net}} = \sigma_{\text{1ion}} + 2\sigma_{\text{2ion}} + 3\sigma_{\text{3ion}} + \dots$ ) and will be benchmarked against the reported experimental and theoretical data in the following section.

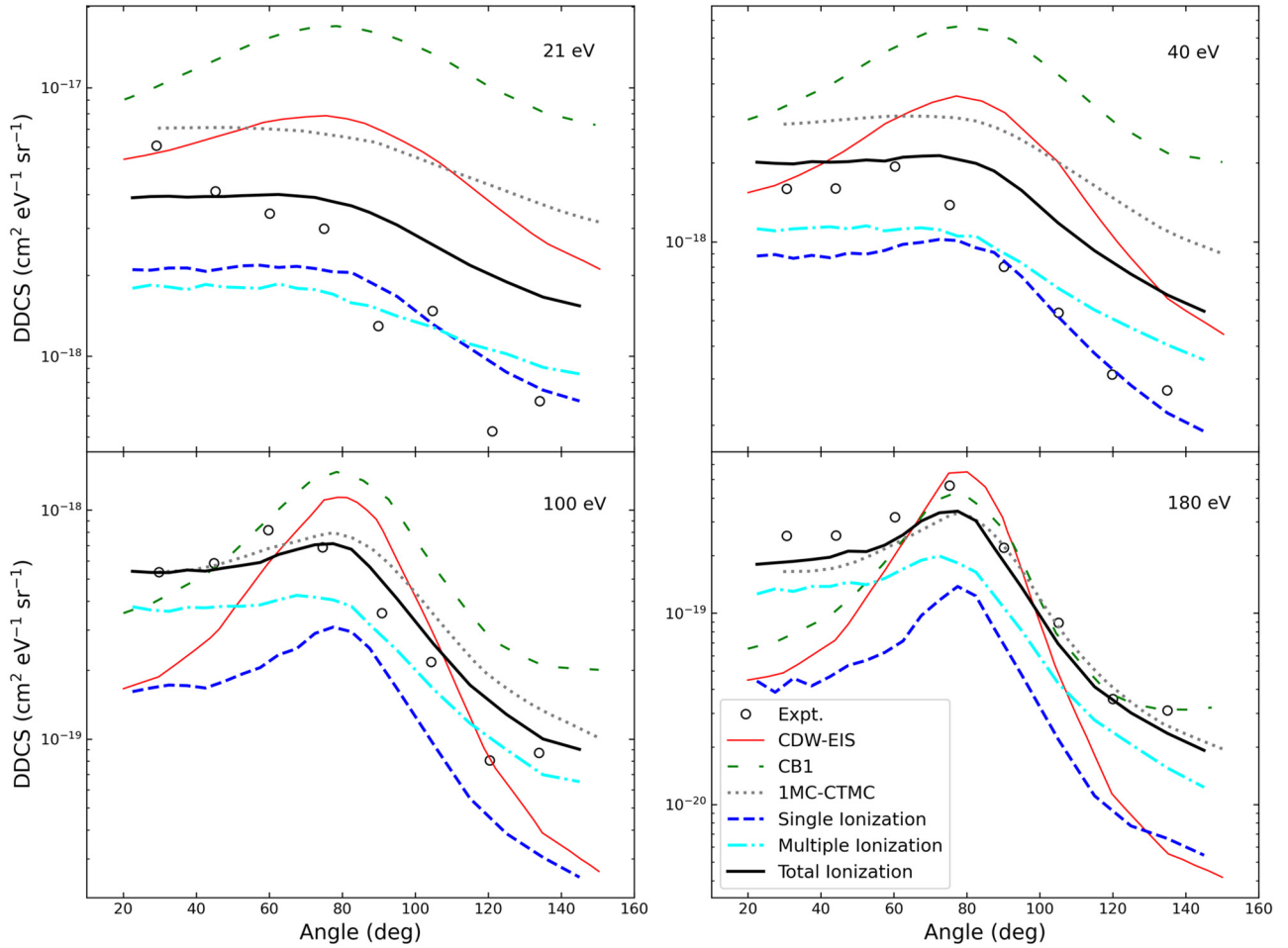


FIG. 5. DDCS as a function of the electron emission angle at different emission energies. Theories and experimental data as in Fig. 3.

### III. RESULTS

First we consider the ionization DDCS as a function of the electron emission energy at specific emission angles for  $C^{6+}$  collisions on uracil at an impact energy of 3.5 MeV/u. Experimental data are those reported by Agnihotri *et al.* [19]. In Fig. 3 we consider electron emission angles of  $30^\circ$ ,  $45^\circ$ ,  $60^\circ$ , and  $75^\circ$ , and in Fig. 4 we consider  $90^\circ$ ,  $105^\circ$ ,  $120^\circ$ , and  $135^\circ$ . From the experimental data we clearly infer the presence of the KLL-Auger peaks for C, N, and O, which are expected at electron emission energies of approximately 240, 355, and 480 eV. The classical simulation procedure previously described does not include the Auger mechanism, which has been separately considered. To our knowledge, there are no specific studies regarding the angular behavior of these Auger peaks for the uracil molecule following ion impact. Based on previous studies of the C and O peaks for  $CO_2$  molecules, we have assumed an isotropic distribution for the three KLL Auger peaks [36]. Total ionization cross sections for the K-shell electrons of C, N, and O obtained using a three-body CTMC code have been convoluted by means of Gaussian functions centered at the respective Auger peak energies with a full width at half-maximum of 30 eV. This value was arbitrarily chosen and leads to a good visual agreement with the reported data at the largest emission angles

considered. These Gaussian peaks were then added to the DDCS calculated within the Ad-CTMC scheme.

Theoretical data previously reported in Ref. [19] obtained by means of the Coulomb-Born 1 (CB1) and the continuum-distorted-wave eikonal initial state (CDW-EIS) are also included, together with the 1MC-CTMC results of Sarkadi [21]. As a general trend, the simplest model (CB1) provides an acceptable description at the lowest emission angle of  $30^\circ$ . However, as the emission angle increases, the results provided by CB1 tend to overestimate the experimental data over the whole energy range explored. In contrast, CDW-EIS results cannot be read so straightforwardly. At the lower emission angles hereby considered, this model provides a very good description of the low-energy region. However, the electronic emission is underestimated for electron energies greater than about 40 eV. As the emission angle increases to  $75^\circ$  and  $90^\circ$ , the model seems to overestimate the data over the whole energy range. Results for angles greater than  $105^\circ$ , clearly show an overestimation of low-energy electrons and an underestimation of energetic electrons. Moving now to the 1MC-CTMC results, we observe that they provide a good description at  $30^\circ$  and  $45^\circ$  but, as the emission angle increases, it tends to overestimate the experimental data.

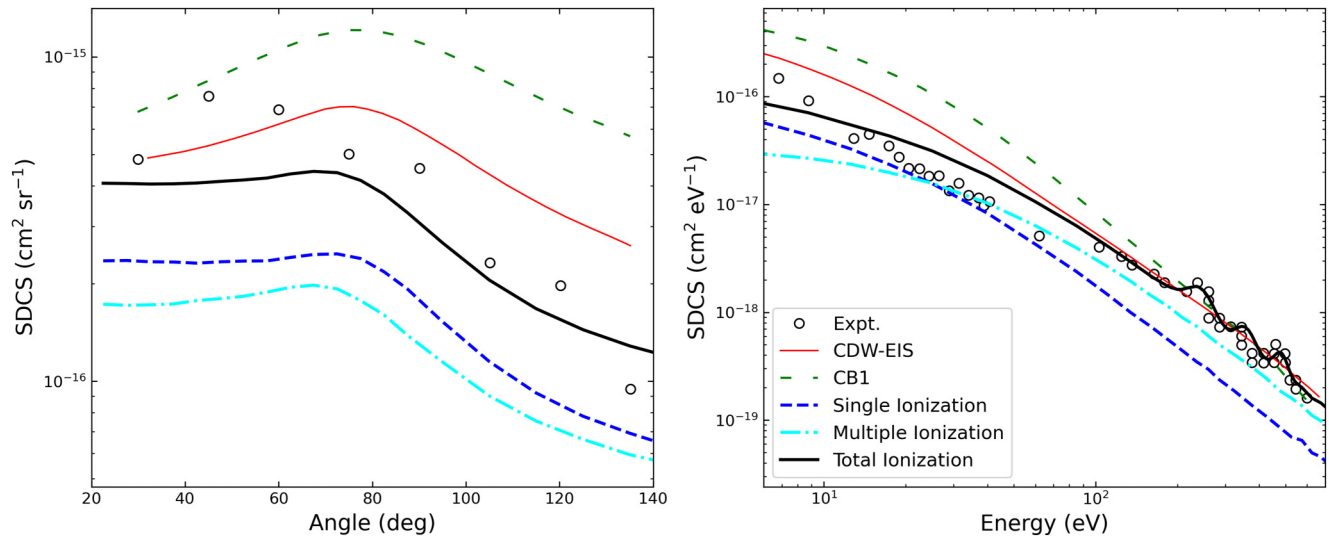


FIG. 6. SDCS as a function of (a) the electron emission angle and (b) electron energy. Theories and experimental data as in Fig. 3.

We now describe the results obtained by means of the present Ad-CTMC method. Separate contributions for the single and multiple ionization channels are explicitly shown together with the total prediction. The latter also contains the KLL Auger peaks contributions as it has been previously described. As a general trend, single ionization dominates the emission at low electron energies while multiple ionization dominates the emission of energetic electrons. The crossing point in the dominance among these mechanisms is observed to vary between about 13 eV and 30 eV, being the former value associated to large emission angles. Overall, the present methodology is in good agreement with the data at the larger emission angles, while it tends to underestimate the low-energy emission at the lower angles considered. This behavior of the Ad-CTMC method at low emission energies has been previously observed for the H<sub>2</sub>O target and attached to the classical  $1/E$  behavior of the cross section, instead of the proper  $\log(E)/E$  provided by quantal descriptions [10,37]. However, it is worth noting that the 1MC-CTMC model provides a much better description in these cases. From Fig. 2, we infer that the geometrical extension of the electron density predicted by 1MC-CTMC for any given orbital exceeds that provided by quantum mechanics and the Ad-CTMC method. In this sense, it could well be that the overall increase of the geometrical cross section provides a compensation for the classical  $1/E$  underestimation of soft electrons. However, further studies should be carried out before a decisive assessment can be made regarding this point.

In Fig. 5, we present DDCS as a function of the emission angle for electron energies of 21, 40, 100, and 180 eV. We notice that the CB1 theory overestimates the data and fails to reproduce the angular asymmetry at the lower emission energies considered (21 and 40 eV), exhibiting a wide structure with a maximum at about 75°. As the impact energy increases the peak structure narrows and it seems to smoothly improve its agreement with the data. At an emission energy of 180 eV the CB1 theory provides a very good description of the data at emission angles greater than about 80°, but underestimates the data at lower emission angles. The CDW-EIS method,

shows a similar profile at 21 and 40 eV but closer to the experiment. However, at impact energies of 100 and 180 eV, the profile turns narrower than that exhibited by the data and a clear underestimation of the low and large angle regions is observed.

In contrast, 1MC-CTMC and the Ad-CTMC exhibit similar angular profiles. The Ad-CTMC is found in closer agreement with the data in all cases explored. Again, the separate contributions of the single and multiple ionization channels are explicitly shown. The role of the multiple ionization channel in terms of the asymmetry of the DDCS can be inferred from these plots, specially at the larger energies considered (100 and 180 eV), where it is clearly dominant.

Singly differential cross sections in terms of emission angle and energy are shown in Fig. 6. The CB1 model overestimates

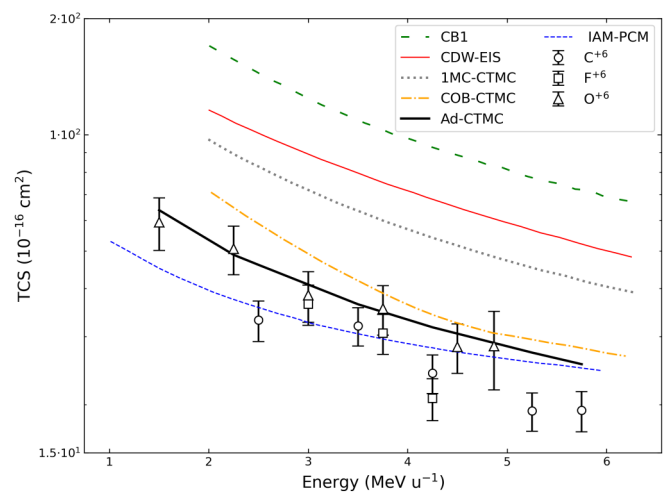


FIG. 7. TCS as a function of the projectile impact energy. Experimental results obtained by Agnihotri *et al.* for C<sup>6+</sup>, O<sup>6+</sup>, and F<sup>6+</sup> projectiles [20,38] are contrasted against theoretical results provided by: CB1, CDW-EIS and COB-CTMC [20]; 1MC-CTMC [21]; IAM-PCM [14]; and the present Ad-CTMC.

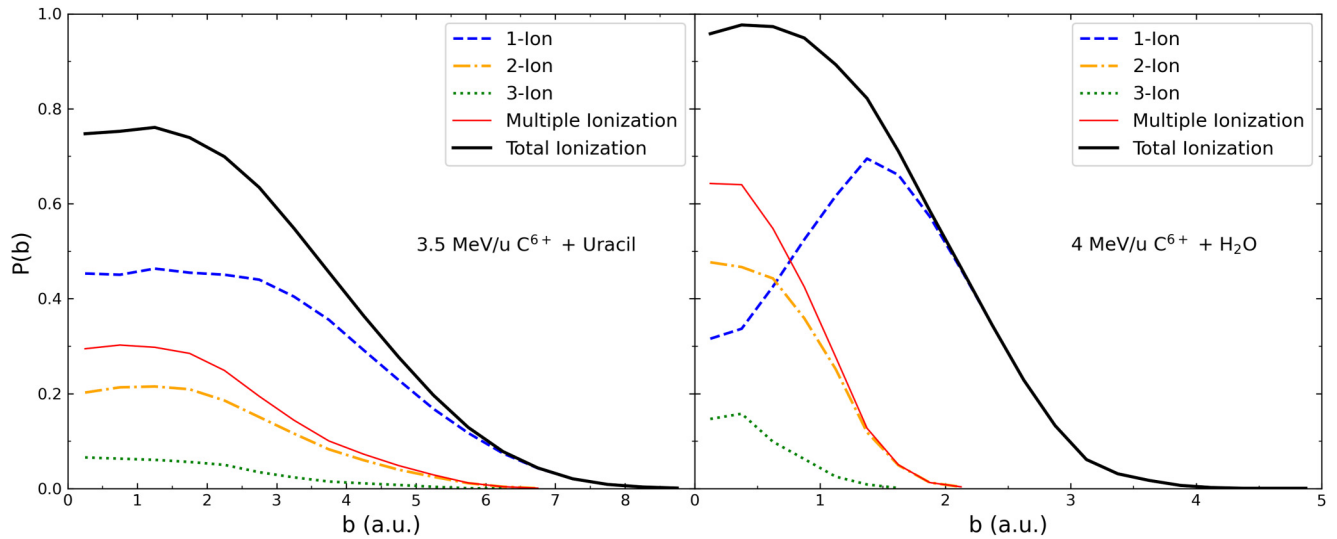


FIG. 8. Single and multiple ionization probabilities as a function of the impact parameter for 3.5 MeV/u  $C^{6+}$  collisions on (a) uracil and 4 MeV/u  $C^{6+}$  collisions on  $H_2O$  previously reported in [10].

the SDCS in angle and is not able to reproduce the angular profile of the experimental data. The CDW-EIS model, on the other hand, leads to SDCS in closer agreement with the data at emission angles lower than  $80^\circ$  but tends to overestimate the data at larger angles. The Ad-CTMC results follow the experimental profile, with an acceptable description over the whole angular range. It can be seen that the dominant contribution is provided by the single ionization channel, highlighting the fact that the low emission energy region is mainly responsible for the SDCS in angle.

Now moving to the SDCS in energy, we observe that the CB1 model clearly overestimates the experimental data for emission energies lower than about 100 eV. The same trend, but to a minor extent, is observed for the CDW-EIS model. The present Ad-CTMC results are in good agreement with the data. At the impact energy explored, the crossing point between the single ionization and the multiple ionization channel is found at about 25 eV.

Total cross sections are shown in Fig. 7, now as a function of the impact energy in the range 2–6 MeV/u. Theoretical predictions are contrasted against the experimental measurements of Agnihotri *et al.* [20,38]. In this case,  $C^{6+}$ ,  $O^{6+}$ , and  $F^{6+}$  projectiles are explicitly considered and help illustrate possible differences between bare and partially stripped projectiles at the impact energy range explored. In this case, the COB-CTMC results of Ref. [20] and the IAM-PCM results of Ref. [14] for a projectile of charge +6 are also added for comparison. As expected, the CB1 model is the one that overestimates the most the TCS, followed in order of increasing proximity to the data by the CDW-EIS, the IMC-CTMC and the COB-CTMC. The IAM-PCM and the present Ad-CTMC results are consistent with the data over the whole energy range explored.

Finally, in Fig. 8 the ionization probability predicted by the Ad-CTMC method as a function of the impact parameter is shown and compared to the results obtained in 4 MeV/u  $C^{6+}$  collisions on  $H_2O$ . Single and multiple ionization contributions are explicitly identified. A clear difference is observed

between both cases. For  $H_2O$ , it was found that single ionization was dominant for impact parameters greater than about 0.7 a.u. while multiple ionization dominated for inner impact parameters. This behavior can be easily understood in terms of the nearly monocentric nature of the  $H_2O$  molecule. In contrast, uracil, a more complex molecule with orbitals extended over different centers, shows a clear dominance of single ionization at all impact parameters. Moreover, and as expected, the single and multiple ionization probabilities for uracil extend to larger  $b$  values.

#### IV. CONCLUSIONS

In this work, a multielectronic multicenter CTMC method recently introduced for ion+ $H_2O$  collisions has been extended to analyze  $C^{6+}$  collisions on uracil. Present results were found in good agreement with the reported experimental data at the total, singly differential, and doubly differential levels.

In agreement with previous analyses for  $H_2O$  targets, present results for uracil suggest that energetic electrons are mostly produced in multiple ionization events, while soft electrons are mainly produced by the single ionization mechanism. Moreover, by analyzing the single and multiple ionization probabilities as a function of the impact parameter, we observed clear differences between uracil and  $H_2O$ . These can be in principle ascribed to the multicentric/monocentric nature of their molecular orbitals.

More experimental studies would be welcome at this point for uracil as well as other DNA bases. These will hopefully help us improve our models and the present state of knowledge regarding these complex collision systems.

#### ACKNOWLEDGMENTS

Work at IFISUR was supported by Grant No. PGI 24/F073, Secretaría General de Ciencia y Tecnología, Universidad Nacional del Sur, and Grant No. PIP 11220170100855CO of CONICET, Argentina.



- [1] T. Liamsuwan and H. Nikjoo, *Phys. Med. Biol.* **58**, 673 (2013).
- [2] A. V. Solov'yov, *Nanoscale Insights into Ion-Beam Cancer Therapy* (Springer International Publishing, Berlin, 2017).
- [3] M. Quinto, J. Monti, C. Tachino, P. Weck, O. Fojón, C. Champion, and R. Rivarola, *Radiat. Phys. Chem.* **167**, 108337 (2020).
- [4] V. B. Tessaro, B. Gervais, F. Poignant, M. Beuve, and M. E. Galassi, *Physica Med.* **88**, 71 (2021).
- [5] P. T. C.-O. Group, Ptcog.ch, <https://www.ptcog.ch/>, 2019, [Online; accessed 31 March 2022].
- [6] T. Liamsuwan and H. Nikjoo, *Phys. Med. Biol.* **58**, 641 (2013).
- [7] S. Bhattacharjee, S. Biswas, J. M. Monti, R. D. Rivarola, and L. C. Tribedi, *Phys. Rev. A* **96**, 052707 (2017).
- [8] S. Bhattacharjee, C. Bagdia, M. R. Chowdhury, J. M. Monti, R. D. Rivarola, and L. C. Tribedi, *Eur. Phys. J. D* **72**, 15 (2018).
- [9] S. Otranto, N. Bachi, and R. E. Olson, *Eur. Phys. J. D* **73**, 41 (2019).
- [10] N. Bachi, S. Otranto, G. S. Otero, and R. E. Olson, *Phys. Med. Biol.* **64**, 205020 (2019).
- [11] N. Bachi, G. S. Otero, S. Otranto, and R. E. Olson, *AIP Conf. Proc.* **2160**, 070006 (2019).
- [12] A. Jorge, M. Horbatsch, C. Illescas, and T. Kirchner, *Phys. Rev. A* **99**, 062701 (2019).
- [13] A. Jorge, M. Horbatsch, and T. Kirchner, *Phys. Rev. A* **102**, 012808 (2020).
- [14] H. J. Lüdde, T. Kalkbrenner, M. Horbatsch, and T. Kirchner, *Phys. Rev. A* **101**, 062709 (2020).
- [15] P. Moretto-Capelle and A. Le Padellec, *Phys. Rev. A* **74**, 062705 (2006).
- [16] M. E. Galassi, C. Champion, P. F. Weck, R. D. Rivarola, O. Fojón, and J. Hanssen, *Phys. Med. Biol.* **57**, 2081 (2012).
- [17] A. Itoh, Y. Iriki, M. Imai, C. Champion, and R. D. Rivarola, *Phys. Rev. A* **88**, 052711 (2013).
- [18] L. Sarkadi, *Phys. Rev. A* **92**, 062704 (2015).
- [19] A. N. Agnihotri, S. Nandi, S. Kasthurirangan, A. Kumar, M. E. Galassi, R. D. Rivarola, C. Champion, and L. C. Tribedi, *Phys. Rev. A* **87**, 032716 (2013).
- [20] A. N. Agnihotri, S. Kasthurirangan, S. Nandi, A. Kumar, C. Champion, H. Lekadir, J. Hanssen, P. F. Weck, M. E. Galassi, R. D. Rivarola, O. Fojón, and L. C. Tribedi, *J. Phys. B: At., Mol. Opt. Phys.* **46**, 185201 (2013).
- [21] L. Sarkadi, *J. Phys. B: At., Mol. Opt. Phys.* **49**, 185203 (2016).
- [22] H. J. Lüdde, M. Horbatsch, and T. Kirchner, *J. Phys. B: At., Mol. Opt. Phys.* **52**, 195203 (2019).
- [23] I. Abbas, C. Champion, B. Zarour, B. Lasri, and J. Hanssen, *Phys. Med. Biol.* **53**, N41 (2008).
- [24] C. Illescas, L. F. Errea, L. Méndez, B. Pons, I. Rabadán, and A. Riera, *Phys. Rev. A* **83**, 052704 (2011).
- [25] L. Meng, C. O. Reinhold, and R. E. Olson, *Phys. Rev. A* **40**, 3637 (1989).
- [26] D. Hennecart and J. Pascale, *Phys. Rev. A* **71**, 012710 (2005).
- [27] C. J. Wood and R. E. Olson, *Phys. Rev. A* **59**, 1317 (1999).
- [28] M. Alessi, N. D. Cariatore, P. Focke, and S. Otranto, *Phys. Rev. A* **85**, 042704 (2012).
- [29] N. D. Cariatore and S. Otranto, *Phys. Rev. A* **88**, 012714 (2013).
- [30] M. W. Schmidt, K. K. Baldridge, J. A. Boatz, S. T. Elbert, M. S. Gordon, J. H. Jensen, S. Koseki, N. Matsunaga, K. A. Nguyen, S. Su, T. L. Windus, M. Dupuis, and J. A. Montgomery Jr, *J. Comput. Chem.* **14**, 1347 (1993).
- [31] C. O. Reinhold and C. A. Falcón, *Phys. Rev. A* **33**, 3859 (1986).
- [32] R. H. Garvey, C. H. Jackman, and A. E. S. Green, *Phys. Rev. A* **12**, 1144 (1975).
- [33] R. E. Olson, J. Ullrich, and H. Schmidt-Böcking, *J. Phys. B: At. Mol. Phys.* **20**, L809 (1987).
- [34] R. E. Olson, J. Ullrich, and H. Schmidt-Böcking, *Phys. Rev. A* **39**, 5572 (1989).
- [35] J. Simcic, D. R. Schultz, R. J. Mawhorter, I. Čadež, J. B. Greenwood, A. Chutjian, C. M. Lisse, and S. J. Smith, *Phys. Rev. A* **81**, 062715 (2010).
- [36] A. Hiltunen, S. Aksela, G. Víkor, S. Ricz, A. Kövér, and B. Sulik, *Nucl. Instrum. Meth. Phys. Res. B* **154**, 267 (1999).
- [37] I. D. Kaganovich, E. Startsev, and R. C. Davidson, *New J. Phys.* **8**, 278 (2006).
- [38] A. N. Agnihotri, S. Kasthurirangan, S. Nandi, A. Kumar, M. E. Galassi, R. D. Rivarola, O. Fojón, C. Champion, J. Hanssen, H. Lekadir, P. F. Weck, and L. C. Tribedi, *Phys. Rev. A* **85**, 032711 (2012).